Research Square

Preprints are preliminary reports that have not undergone peer review.
They should not be considered conclusive, used to inform clinical practice,
or referenced by the media as validated information.

ID3 inhibits the HSV-1 replication through the ROS/ID3/Wnt signaling axis in the pathogenesis of herpes simplex keratitis

Na Chen
Wenzhe Wang
Hu Meng
Yue Wang
Yumeilan Liu
Huanhuan Xu
Jie Yin
Wei Ye
yewei1987320126.com

Yirui Ge

Research Article

Keywords: HSV-1, reactive oxygen species, ID3, Wnt/β-catenin pathway

Posted Date: April 17th, 2026

DOI: https://doi.org/10.21203/rs.3.rs-9074035/v1

License: This work is licensed under a Creative Commons Attribution 4.0 International License.
Read Full License

Additional Declarations: No competing interests reported.

Abstract

Herpes simplex virus type 1 (HSV-1) is a widespread pathogen affecting a large global population. HSV-1 infection can induce herpes simplex keratitis (HSK), a leading cause of vision loss. Current therapeutic approaches remain limited in efficacy. Consequently, investigating novel pathogenic mechanisms is essential for developing improved treatment strategies. Whether reactive oxygen species (ROS) regulates HSV-1 infection in corneal epithelial cells (CECs) through the DNA-binding protein inhibitor ID3 (ID3), and the underlying mechanism, has not been previously reported.

This study demonstrated that HSV-1 infection elevates ROS levels and apoptosis in both human CECs and HSK mouse models. The antioxidant N-acetylcysteine (NAC) reversed these effects. Whole-transcriptome sequencing, RT-qPCR, and immunofluorescence analyses revealed that ID3 expression increased in NAC-pretreated human CECs and HSK mouse models. Overexpression of ID3 suppressed ROS accumulation, HSV-1 replication, and apoptosis in infected CECs, as confirmed by western blotting, flow cytometry, immunofluorescence, and in-cell western assays. Furthermore, ID3 overexpression downregulated the Wnt/β-catenin signaling pathway, which correlated with reduced HSV-1 replication and diminished apoptosis in CECs.

In HSV-1-infected CECs, elevated ROS promotesHSV-1 replication and apoptosis by inhibiting ID3 expression, thereby activating the Wnt/β-catenin signaling pathway. These findings identify ID3 as a promising therapeutic target for HSK.

1. Introduction

HSV-1 is a neurotropic virus characterized by double-stranded DNA which is responsible for severe eye diseases and encephalitis[1, 2]. HSV-1 is the type of herpes simplex virus with the largest number of human infections. According to the latest 2020 WHO statistics, approximately 3.8 billion people aged 0–49 are positive for the HSV-1 serotype[3]. Based on this data, it is estimated that if the remaining population of other age groups is included, the number of HSV-1 serotype-positive patients may reach 5 billion[4]. HSV-1 can widely infect the tissues of the eye, such as the cornea, eyelids and retina[5]. Herpes simplex keratitis is caused by direct contact of HSV-1 with the ocular mucosa. HSK can be classified into various types based on different clinical manifestations, epithelial dendritic lesions predominate 56.3%, stromal keratitis 29.5%, and geographic epithelial lesions 9.8% [6]. HSK infection initially invades corneal epithelial cells, and many patients also present with corneal epithelial inflammation as the initial symptom[7]. HSK can cause eye pain, photophobia and vision loss. has a reported It is reported that the incidence rate of HSK is approximately 149 per 100,000 population. The incidence rate is higher in underdeveloped areas [8]. Among HSK patients, approximately half of them have relapses, and the number of patients with relapses of 6 to 15 times exceeds[8, 9]. Therefore, keratitis caused by HSV-1 infection is one of the main causes of blindness in patients. At present, there is no completely effective treatment for HSK, so it is extremely necessary to identify potential therapeutic targets.

previous studies have shown that after infecting host cells, HSV-1 can cause the accumulation of ROS within the cells[10]. Studies have shown that mitochondrial damage and the reduction of antioxidant enzymes are the main reasons for the increase of ROS in host cells infected with HSV-1[11, 12]. HSV-1 infection increased ROS levels as early as 1 h post infection and ROS levels remained elevated at 24 h post-infection (hpi) in neural cells[13]. Excessive accumulation of ROS can lead to cell apoptosis, thereby causing the occurrence of various diseases. The ROS can also significantly impact viral replication[10]. In our previous study, they also find that ROS/JAG1 signaling pathway mediates CECs apoptosis in herpes simplex keratitis by suppressing autophagy[14]. In previous studies, it was believed that the ROS induced by HSV-1 was the main cause of apoptosis in host cells[15, 16]. However, there are many controversies regarding the effect of ROS on viral replication in host cells, and the mechanism remains unclear.

ID3 is a transcriptional regulator that negatively controls basic helix–loop-helix transcription factors by forming heterodimers and inhibiting their DNA-binding and transcriptional activity[17, 18]. ID3 is induced by many factors, including: TGF-β[19], cAMP[20], angiotensin II[21] and plays different roles depending on the cell type. Studies have shown that ID3 is closely related to the generation of ROS and the antioxidant process. During the process of vascular proliferation induced by estrogen, ROS can promote the phosphorylation of ID3, thereby triggering the proliferation of blood vessels [22]. In immortalized keratinocytes, UVA irradiation leads to an increase in ROS levels, as well as an increase in the expression of ID3 mRNA. The increased ID3 induces the expression of the pro-apoptotic BAX protein, resulting in an increase in cell apoptosis[23]. At present, the effects and mechanisms of ID3 on cell apoptosis and viral replication in HSV-1-infected corneal epithelial cells remain unclear.

The processes of HSV-1 infection and replication are closely related

to the signaling pathways involved in cellular molecular synthesis, metabolism, growth, and survival. In our previous studies, it was found that Wnt/β-catenin was activated in both HSV-1-infected corneal epithelial cells and HUVECs cells [24, 25]. Further research has revealed that the Wnt/β-catenin pathway is a crucial pathway that promotes angiogenesis, cell apoptosis and viral replication. Studies have shown that in patients with metastasis of intrahepatic cholangiocarcinoma, ID3 can increase the transcriptional activity of β-catenin, thereby promoting the metastasis of intrahepatic cholangiocarcinoma[26]. During the development of mammalian embryos, ID3 can promote embryonic development by activating the Wnt signaling pathway[27]. At present, the regulatory mechanism between the ID3 and Wnt signaling pathways after HSV-1 infects host cells remains unclear.

In this study, we aimed to determine whether ROS plays a role in the replication of HSV-1 in corneal epithelial cells and how the mechanism works. We found that ROS was upregulated in HSV-1 infected CECs. After treatment with the antioxidant NAC, the ROS levels in HSV-1 infected CECs decreased, and the replication of HSV-1 virus was reduced. Further studies revealed that ROS inhibited the expression of ID3, thereby activating the Wnt/β-catenin signaling pathway, which in turn promoted the replication of HSV-1 virus. Thus, ID3 is a potential therapeutic target for HSV-1 infection in CECs.

2. Materials and methods

2.1. Cells and viruses

The human corneal epithelial cells (ATCC, Manassas, VA, USA) were cultured in DMEM/F12 (Gibco, USA) supplemented with 10 % fetal bovine serum (FBS, Gibco, USA) and 1 % penicillin/streptomycin solution (Gibco, USA) in a humidified, 37℃, 5 % CO_2 incubator. The HSV-1 F strain was kindly provided by Professor Zhiwei Wu from the Center for Public Health Research at Nanjing University Medical School.

A N-acetyl-L-cysteine (NAC; MCE, China) was dissolved in PBS to concentrations of 5 and 10 mM for treatment in *vitro*.

2.2. Cell transfection

The human CECs were cultured in 6-well plates and transfected at 60 –80% confluence via liposomal transfection method. The human-derived overexpression plasmid pCMV3-SV40-ID3(Corues biotechnology, China) were transfected with Lipofectamine 3000 (Thermo Fisher Scientific, China) following the manufacturer's protocols.

2.3. Animals and HSK mice model

Six-week-old male C57BL/C mice were purchased from Nanjing Hui miao xin Biotechnology Co., Ltd (Nanjing, China). All the mice were raised in an clean environment of approximately 25 ℃ and 12 hours of day/night cycle. All mice are allowed free access to food and water. Animal experiments were approved by the Institutional Animal Care and Use Committee of Jinling Hospital and conducted in concordance to the guidelines of Association for Research in Vision and Ophthalmology (ARVO) for the use of animals in Ophthalmic and Vision Research.

HSK mice model and HSK score for corneal opacity was consistent with the treatment in our previous articles [24]. Mice in the NAC groups were treated with eye drops of NAC (0.3%, 5 μL/ eye, three times per day) for 3 continuous days.

Adeno-associated virus (AAV) injection: Mice were assigned to four groups: CON, HSK, HSK + AAV-NC and HSK + AAV-ID3 (Corues biotechnology, China). AAV-ID3 or AAV-NC (5 μl, titres ≥1 × 10^{12}) was administered subconjunctival one week before HSV-1 infection.

2.4. Western blotting

Cells collected were lysed with RIPA lysis buffer (New Cell) to extract the total protein solution. 20 μg of the protein sample was added to a 8–12 % SDS-PAGE gel (Beyotime, China) for electrophoresis to separate proteins. The separated proteins in the gel were transferred to a PVDF membrane (Merck, Germany). The membrane was treated with 5% skim milk blocking solution. The membrane was incubated overnight at 4°C with a specific primary antibody. The membrane was incubated with an

enzyme-labeled secondary antibody at room temperature for 1 hour. The washed protein bands were visualized by adding ECL Western Blotting Detection Reagent and using a Gel imaging system. Protein expression was normalized to GAPDH. ImageJ software (National Institutes of Health, USA) was used to calculate the relative expression level of the target protein. The antibodies used in this study can be found in Table1.

Table1. Information of Antibodies

Name	Catalog Number	Source	Manufacturer	Country	Applications
GAPDH	10494-1-AP	Rabbit	Proteintech	C.N	WB
ICP0	sc-53070	Mouse	Santa Cruz	USA	WB
ICP4	sc-69809	Mouse	Santa Cruz	USA	WB
HSV-1 gD	sc-21719	Mouse	Santa Cruz	USA	WB, IF
BAX	60267-1-Ig	Mouse	Proteintech	C.N	WB
Bcl2	26593-1-AP	Rabbit	Proteintech	C.N	WB
ID3	9837	Rabbit	CST	USA	WB, IF
ID3	F2652	Rabbit	Selleck	USA	IP
LRP6	HA600065	Mouse	HUABIO	C.N	IP
LRP6	ab134146,	Rabbit	Abcam	Uk	WB
β-catenin	66379-1-Ig	Mouse	Proteintech	C.N	WB, IF
HRP-conjugated anti-rabbit	SA00001–2	Goat Anti-Rabbit	Proteintech	CN	WB
HRP-conjugated anti-mouse	SA00001–1	Goat Anti-Mouse	Proteintech	CN	WB
CoraLite594-conjugated	SA00013–4	Goat Anti-Rabbit	Proteintech	CN	IF
CoraLite488-conjugated	ab150077	Goat Anti-Mouse	Proteintech	CN	IF

2.5. High-throughput RNA sequencing

Total RNA was extracted from HSV-1 infected human CECs and NAC pretreated- HSV-1 infected 24 hpi using the TRIzol reagent (Sangon Biotech, China). The concentration and purity of the total RNA sample were measured using a Nanodrop 1000 (Thermo Scientific, USA).

The methods of whole transcriptome sequencing and differential gene analysis were consistent with our previous studies[14, 24].

2.6. Quantitative real-time polymerase chain reaction (RT–qPCR)

Extract total RNA from the samples using FreeZol Reagent (Vazyme, China), measure the RNA concentration. Reverse transcribes the total RNA of the samples into cDNA. Use the SYBR Green method, perform amplification cycles on the real-time fluorescence quantitative PCR instrument (ABI, USA) and collect fluorescence signals in real time.

Calculate the expression change ratio of the target gene relative to the reference gene using $2^{-\Delta\Delta Ct}$ method, with GAPDH utilized as a reference gene. The primer sequences employed for gene expression analysis can be found in Table 2.

Table 2. List of primer sequence for RT-qPCR

Gene	Primer sequences (5'→3')
ID3	F: AGCTTGCTGGACGACATGAA
	R: GTAGTCGATGACGCGCTGTA
GAPDH	F: GGAGCGAGATCCCTCCAAAAT
	R: GGCTGTTGTCATACTTCTCATGG
ID3（mouse）	F: TGCGAGAGGGAGCCAGACC
	R:GGTTAGGAGACGAGTTAGCCAAGG
GAPDH(mouse)	F:TGATGACATCAAGAAGGTGGTGAAG
	R:TCCTTGGAGGCCATGTGGGCCAT

2.7. Immunofluorescence staining

Cells were cultured and treated in confocal dishes. Samples were fixed with 4% paraformaldehyde solution (Solarbio, China) at room temperature for 30 minutes and washed three times with PBS buffer. Primary antibodies diluted 1:100 with a mixture of 1% Triton X-100 and 2% BSA were added to the samples and incubated overnight at 4°C. Fluorescently labeled secondary antibodies diluted 1:200 with a mixture of PBS buffer were incubated with the samples in the dark at 37°C for 1 hour. The samples treated with anti-fluorescence quenching solution containing 4,6-diamidino-2-phenylindole (DAPI) (Beyotime, China), and the localization and expression of the target protein were observed under Laser Scanning Confocal Microscope (LSM 980, Carl Zeiss Microscopy GmbH, Germany).

2.8. Immunofluorescence staining of mice corneal tissues

After the corneal tissue sections were subjected to paraffin sectioning, dewaxing and antigen retrieval procedures, and then treated with a mixture of 0.5% Triton X-100 and 2% BSA for permeabilization and blocking. The samples were incubated with primary antibodies diluted 1:100 in a mixture of 0.5% Triton

X-100 and 2% BSA at 4°C overnight. The samples were incubated with secondary antibody diluted 1:500 in PBS in the dark at 37°C for 1 hour. The samples treated with anti-fluorescence quenching solution containing DAPI, and the localization and expression of the target protein were observed under Laser Scanning Confocal Microscope.

2.9. TUNEL staining

The paraffin sections of the corneal tissues of HSK mice were stained with Terminal deoxynucleotidyl transferase-mediated dUTP nick-end labeling (TUNEL) according to the instructions of the TUNEL assay kit (Vazyme Biotech, China). The staining was visualized and captured using Laser Scanning Confocal Microscope (LSM 980, Carl Zeiss Microscopy GmbH, Germany).

2.10. In-Cell Western Blotting

Human CECs were cultured in a 96-well plate. Fix the samples at room temperature with 4% paraformaldehyde for 30 minutes. Treat the samples 1% Triton X-100 and 2% BSA mixed solution for 30 minutes at room temperature. Incubate primary antibody with a 1% Triton X-100 and 2% BSA mixed solution at a ratio of 1:200 with the cells at 4°C overnight. Incubate the DYLight 800 conjugate IgG (1:1000) fluorescent dye directly with the cells at room temperature for 1 hour, then wash three times with PBS buffer; add DRAQ5 (1:500) and incubate at room temperature for 15-30 minutes. The images were visualized and captured by the NIR near-infrared laser (Azure Biosystems, USA), according to the manufacturer's instructions.

2.11. Flow cytometry analysis

Human CECs were cultured and treated in a 6-well plate. The cells were collected and washed twice with pre-cooled PBS. The single-cell suspension was treated by the Annexin V-FITC/PI Apoptosis Detection Kit (Vazyme Biotech, China) as the manufacturer's instructions. Then the treated human CECs measured using a BriCyte E6 flow cytometer (Mindray, China). The data were analyzed using the FlowJo V10.0 software (FlowJo, USA).

2.12. ROS detection

We assessed intracellular ROS levels of human CECs with 10μL of 2',7'-dichlorodi-hydrofluorescein diacetate (DCFH-DA) (MCE, USA) dye (1:1000 dilution) for half 1 hour at 37 ˚C. Subsequently, the cells were washed with PBS buffer and then subjected to fluorescence microscopy photography and flow cytometry staining experiments respectively.

2.13. Molecular docking for LRP6/ID3 and core targets

Protein-protein molecular docking was performed between LRP6 and ID3 using the GRAMM-X (https://gramm.compbio.ku.edu/) and HDOCK (http://hdock.phys.hust.edu.cn/) platforms to analyze potential interaction sites. The protein structure PDB files of LRP6 (Entry: O75581) and ID3 (Entry:

Q02535) were downloaded from the Uniport (https://www.uniprot.org/) database. Then, both structural files were subsequently uploaded to GRAMM-X and HDOCK for docking calculations.

The resulting docking models were submitted to Protein-Ligand Interaction Profiler(https://www.ebi.ac.uk/pdbe/pisa/) for interaction analysis. Finally, the top-ranking docking models from both GRAMM-X and HDOCK were visualized using Pymol 2.3.0.

2.14. Co-IP and immunoprecipitation (IP) assay

Wash the cells twice with PBS. According to the manufacturer's instructions for the Universal IP/Co-IP Toolkit (Magnetic Beads) (Abbkine, China), add 1 mL of pre-chilled non-denaturing lysis buffer supplemented with protease and phosphatase inhibitors to the cells, followed by cell lysis at 4°C for 1 hour. Centrifuge the lysate at 12,000 rpm and 4°C for 10 minutes using a low-temperature centrifuge, collect the supernatant, and determine the protein concentration via the BCA assay.For the input group: Aliquot 40–50 μL of the protein sample supernatant from both the control and treatment groups, add 5× loading buffer, heat at 100°C for 10 minutes, and store at -80°C.For magnetic bead preparation and antibody conjugation: Transfer 20 μL of Protein A/G Magnetic Beads into a 1.5 mL centrifuge tube, place the tube on a magnetic separation rack, let stand for 10 seconds, and aspirate the supernatant. Wash the Protein A/G Magnetic Beads three times with wash buffer. Add 1 μg of primary antibodies (Mouse IgG, Rabbit IgG, LRP6, ID3) to resuspend the beads, then incubate at 4°C for 12 hours on a vertical rotating mixer. After incubation, place the tube on the magnetic separation rack, let stand for 10 seconds, and wash the antibody-conjugated Protein A/G Magnetic Beads. For immunoprecipitation (IP): Add 1 mg of protein sample to each group of antibody-conjugated Protein A/G Magnetic Beads, and incubate at room temperature for 1 hour on a vertical rotating mixer. Place the tube on the magnetic separation rack, let stand for 10 seconds, add 1 mL of wash buffer, resuspend, and wash the beads three times. Elution and sample preparation for detection: Add 50 μL of 1× SDS-PAGE loading buffer to the tube, heat at 100°C for 10 minutes, centrifuge at 12,000 rpm for 10 minutes, and collect the supernatant as the IP group. Subject the samples to sodium dodecyl sulfate-polyacrylamide gel electrophoresis (SDS-PAGE) and Western blotting analysis. The antibodies used in this study can be found in Table1.

2.15. Statistical analysis

GraphPad Prism 8 (GraphPad, Bethesda, MD) was used for data analysis and visualization. Statistical differences between groups were analyzed using Student's *t*-test for two groups, one-way and two-way ANOVA for multiple groups. The results were expressed as mean ± standard deviation (SD). Significant differences were accepted at $P \leq 0.05$ in all analyses.

3. Results

3.1 ROS level and apoptosis of the CECs increased after infected by HSV-1 in vitro and in vivo

Based on our previous research, human CECs were infected with HSV-1 (MOI = 0.5) for 24 hours. After 24 hpi, the expression of the HSV-1 infection-related viral proteins ICP0, ICP4, and HSV-1 gD were increased in HSV-1 infected group by western blot assays (Fig. 1A and B). The In-Cell Western assay further confirmed the elevated expression of HSV-1 gD protein following infection (Fig. 1B). Flow cytometry indicated that HSV-1 infection promoted HCEC apoptosis (Fig. 1C and D). Using DCFH-DA staining, we observed a significant increase in ROS levels in HSV-1-infected human CECs, as assessed by fluorescence microscopy and flow cytometry (Fig. 1E, F, and G). Three days after inoculating mouse corneas with HSV-1, anterior segment photography and sodium fluorescein staining showed corneal damage in HSK mice, with significantly higher corneal epithelial scores (Fig. 1H and I). The TUNEL assay further demonstrated increased apoptosis of corneal epithelial cells in the corneas of HSK mice (Fig. 1J).

These findings indicate that HSV-1 infection induces corneal epithelial cell apoptosis and elevates intracellular ROS levels both in *vitro* and in *vivo*.

(A–G) Human CECs were infected by HSV-1(MOI = 0.5) for 24 h. (A) Representative western blot showing ICP4, ICP0 and HSV-1 gD protein expression. (B) Statistical chart of A (n = 3). (C) Flow cytometry staining results of apoptosis. (D) Statistical chart of B (n = 3). (E) Representative immunofluorescence staining by DCFH-DA (bars = 100 μm). (F) Flow cytometry staining results of ROS generation. (G) Statistical chart of F (n = 3). (H) Typical images of mice corneal and fluorescein sodium staining images taken on 3 dpi. (I) Statistical chart of HSK score (n = 3). (J) TUNEL staining of mice corneal sections on 3 dpi. TUNEL staining (red) and DAPI (blue). Bars = 100 μm. **P* < 0.05, ***P* < 0.01, ****P* < 0.001 and *****P* < 0.0001 versus the CON group.

3.2 NAC can inhibit HSV-1 replication, ROS level and apoptosis of HSV-1 infected CECs in vitro and in vivo

To investigate the effect of ROS on HSV-1 replication in Human CECs, we pretreated the cells with the intracellular ROS scavenger NAC at two concentrations (5 mM and 10 mM) for one hour prior to HSV-1 infection.

Fluorescence microscopy (Fig. 2A) and flow cytometry (Fig. 2B, C) revealed that HSV-1 infection significantly increased ROS levels at 24 hpi, an effect that NAC pretreatment markedly suppressed. NAC pretreatment also reduced the expression of the HSV-1 related viral proteins ICP0, ICP4, and gD compared with the HSV-1 infected group (Fig. 2D, E). In-cell western assays further confirmed that HSV-1 gD protein expression was lower in NAC-pretreated cells than in infected controls (Fig. 2F). Flow cytometry indicated that NAC inhibited the HSV-1 promoted apoptosis of human CECs (Fig. 2G, H). Consistent with our earlier findings, NAC treatment significantly reduced both fluorescein sodium staining and clinical HSK scores in mice at 3 dpi (Fig. 2I, J). TUNEL assays additionally showed that NAC decreased apoptosis in the corneal epithelium of HSK mice (Fig. 2K).

These results demonstrate that HSV-1 infection elevates ROS levels, viral replication, and apoptosis in CECs, all of which were significantly attenuated by NAC treatment both in *vitro* and in *vivo*.

Figure 2. NAC can inhibit HSV-1 replication, ROS level and apoptosis of HSV-1 infected CECs in vitro and in vivo

(A–G) Human CECs were infected by HSV-1(MOI = 0.5) for 24 h. Human CECs were pretreated by different concentration of NAC (N1 = 5 Mm and N2 = 10 Mm), then HSV-1 infected human CECs for 24 hours. (A) Representative immunofluorescence staining by DCFH-DA (bars = 100 μm). (B) Flow cytometry staining results of ROS generation. (C) Statistical chart of B (n = 3). (D) Representative western blot showing ICP4, ICP0 and HSV-1 gD protein expression. (E) Statistical chart of D (n = 3). (F) In cell western blot analysis was used to identify the viral protein HSV-1 gD (green), which was normalized by DRAQ5 (red). (G) Flow cytometry staining results of apoptosis. (H) Statistical chart of G (n = 3). (I-K) Mice in the NAC group were treated with NAC eye drops (0.3%, 5 μL/ eye, three times daily) for 3 continuous days (I) Typical images of mice corneal and fluorescein sodium staining images taken on 3 dpi. (J) Statistical chart of HSK score (n = 3). (K) TUNEL staining of mice corneal sections on 3 dpi. TUNEL staining (red) and DAPI (blue). Bars = 100 μm. **P* < 0.05, ***P* < 0.01, ****P* < 0.001 and *****P* < 0.0001.

3.3 ID3 expression in CECs and corneal tissues after infected with HSV-1 and treated by NAC

Whole transcriptome sequencing at 24 hpi identified differentially expressed genes between HSV-1(MOI = 0.5)-infected human CECs and those pretreated with 5 mM NAC. Differentially expressed genes were selected based on the criteria of $|\log2FC| \geq 1$ and $q < 0.05$. This analysis revealed 225 upregulated and 353 downregulated genes. Both the volcano plot and heatmap demonstrated a marked increase in ID3 expression in the NAC-pretreated group relative to the HSV-1-infected group (Fig. 3A, B). Gene Ontology and KEGG enrichment analyses further suggested that the differentially expressed genes may regulate the Wnt signaling pathway, apoptotic processes, and HSV-1 infection in human CECs (Fig. 3C, D). Collectively, the transcriptome data indicated that ID3 expression was substantially elevated in NAC-pretreated human CECs at 24 hpi. RT-qPCR analysis confirmed that ID3 expression was significantly higher in the NAC-pretreated group than in the HSV-1-infected group at 24 hpi (Fig. 3E). Western blot and immunofluorescence assays also showed increased ID3 levels alongside decreased HSV-1 gD protein expression in NAC-pretreated human CECs at the same time point (Fig. 3F–H). In a murine HSK model, ID3 expression was reduced in corneal epithelial cells on day 3 post-infection, whereas topical administration of 5 nM NAC restored ID3 levels and suppressed HSV-1 gD expression, as evidenced by RT-qPCR (Fig. 3I) and immunofluorescence (Fig. 3J).

These results imply that ID3 expression and its associated signaling pathways may contribute to the anti-HSV-1 activity of NAC in corneal epithelial cells.

Whole transcriptome sequencing between the HSV-1(MOI = 0.5)-infected and 5 Mm NAC pretreated HSV-1(MOI = 0.5) infected group at 24 hpi. (A–J) Whole transcriptome sequencing between the HSV-1(MOI = 0.5)-infected and 5 Mm NAC pretreated HSV-1(MOI = 0.5) infected group at 24 hpi. (A) Volcano plot of whole transcriptome sequencing data, upregulated genes (red) while downregulated genes (blue) Grey non-significantly different (Grey). (B) Heat map of different expression genes clustering. Red indicates upregulation, and blue indicates downregulation. (C) Scatter plot of GO for different expression genes in different classifications. (D) Bar plot of KEGG enrichment pathway. (E) Relative expression of ID3 mRNA level (n = 3). (F) Representative western blot showing the ID3 protein expression. (G) Statistical chart of F. (H) Representative immunofluorescent staining of HSV-1 gD (red), ID3 (green) and DAPI (blue) in human CECs. Bars = 50 μm. (I) Relative expression of ID3 mRNA level in mice cornea (n = 3). (J)Immunofluorescent staining of ID3 (red), HSV-1 gD (green) and DAPI (blue) of mice corneal tissues. Bars = 100 μm.$^{**}P < 0.05$, $^{**}P < 0.01$ and $^{ns}P > 0.05$.

3.4 ID3 overexpression can inhibit the replication of HSV-1 in CECs

To investigate the role of ID3 in HSV-1-infected CECs, we overexpressed ID3 in human CECs using plasmid transfection. RT-qPCR (Fig. 4A) and Western blot (Fig. 4B and 4C) confirmed the overexpression efficiency. Western blot analysis showed that HSV-1 infection increased the levels of viral proteins ICP0, ICP4, and HSV-1 gD, while ID3 overexpression significantly reduced their expression (Fig. 4D and 4E). Consistent with these findings, in cell western blot assays (Fig. 4F) and immunofluorescence staining (Fig. 4G) also demonstrated decreased HSV-1 gD expression in ID3 overexpression group.

Subconjunctival injection of AAV was performed to overexpress ID3 in mouse corneal tissue, followed by corneal infection with HSV-1 virus one day later. In HSK mice model, ID3 expression was reduced in corneal epithelial cells on day 3 post-infection, whereas AAV-ID3 overexpressed ID3 levels in ID3group (Fig. 4J). Overexpression of ID3 can significantly reduce corneal epithelial damage caused by HSV-1 infection in the cornea (Fig. 4H and 4I). Further studies have found that overexpression of ID3 can inhibit the expression of HSV-1 gD in corneal epithelial of HSK mice. (Fig. 4J).

In summary, ID3 attenuates HSV-1 replication in HSV-1-infected CECs both in *vitro* and in *vivo*.

(A-I) ID3 was overexpressed in human CECs using plasmids. (A)Relative mRNA levels of ID3 (n = 3). (B) Representative western blot showing ID3 protein expression. (C) Statistical chart of B (n = 3). (D) Representative western blot showing ICP4, ICP0 and HSV-1 gD protein expression. (E) Statistical chart of D (n = 3). (F) In cell western blot analysis was used to identify the viral protein HSV-1 gD (green), which was normalized by DRAQ5 (red). (G) Representative immunofluorescent staining of HSV-1 gD (red), ID3 (green) and DAPI (blue) in human CECs. Bars = 50 μm. (H) Typical images of mice corneal and fluorescein sodium staining images taken on 3 dpi. (I) Statistical chart of HSK score (n = 3).(J) Immunofluorescent staining of ID3 (red), HSV-1 gD (green) and DAPI (blue) of mice corneal tissues. Bars

= 100 μm.. * versus CON group, # versus HSV-1 + NC group *$p < 0.05$; **$p < 0.01$; ***$p < 0.001$; ****$p < 0.0001$ and ^{ns} $P > 0.05$.

3.5 ID3 overexpression can inhibit apoptosis and ROS level in CECs

We also found that HSV-1 can cause apoptosis of CECs. After overexpression of ID3, flow cytometry confirmed that the number of apoptotic human CECs decreased (Fig. 5A and 5B). After overexpression of ID3, the western blot results showed that the expression level of pro-apoptotic protein BAX decreased, while the expression level of anti-apoptotic protein Bcl2 increased (Fig. 5C and 5D). The TUNEL assay further demonstrated increased apoptosis of corneal epithelial cells in the corneas of HSK mice can be reversed by overexpression of ID3 (Fig. 5E).

DCFH-DA staining analyzed by and flow cytometry (Fig. 5F and 5G) and fluorescence microscopy (Fig. 5H) revealed that ID3 overexpression suppressed the elevated ROS levels induced by HSV-1 infection. These results indicate that ID3 regulates ROS generation.

In summary, ID3 attenuates HSV-1 replication in HSV-1-infected CECs both in *vitro* and in *vivo*.

(A) Flow cytometry staining results of apoptosis in CECs. (B) Statistical chart of A (n = 3). (C) Representative western blot analysis of apoptosis-related proteins BAX and Bcl-2. (D) Statistical analysis of (n = 3). (E) TUNEL staining of mice corneal sections on 3 dpi. TUNEL staining (red) and DAPI (blue). Bars = 100 μm. (F) Flow cytometry staining results of ROS generation. (G) Statistical chart of F (n = 3). (H) Representative immunofluorescence staining by DCFH-DA (bars = 100 μm). * versus CON group, # versus HSV-1 + NC group *$p < 0.05$; **$p < 0.01$; ***$p < 0.001$; ****$p < 0.0001$ and ^{ns} $P > 0.05$.

3.6 ID3 inhibits HSV-1 replication via the ID3/Wnt signaling pathway in CECs

To investigate how ID3 regulates HSV-1 infection in CECs, we identified Wnt signaling as a potential downstream pathway of ID3 using GO and KEGG analysis of differentially expressed genes from our transcriptome sequencing data (Fig. 3D). Our previous studies have already established the involvement of Wnt signaling in HSV-1-infected CECs[24].

In this study, in order to confirm the interaction relationship between ID3 and LRP6. Protein-protein molecular docking was performed between LRP6 and ID3 by GRAMM-X and HDOCK. We found that the ID3 and LRP6 proteins have multiple amino acid and hydrogen bond binding sites (Fig. 6A). Additionally, we performed Co-IP and immunoprecipitation studies and found that endogenous ID3was pulled down with LRP6 protein, suggesting that ID3, which contains the binding domains of LRP6, is sufficient for interaction with LRP6(Fig. 6B). In infected cells, the expression levels of the Wnt signaling pathway proteins LRP6 and β-catenin were upregulated. Overexpression of ID3, however, downregulated the expression of both LRP6 and β-catenin (Fig. 6C-E).

These results indicate that ID3 inhibits HSV-1 replication in CECs via the Wnt signaling pathway.

(A) Three-dimensional molecular docking model of ID3 with LRP6, showing the predicted binding interface. (B) Co-IP and immunoprecipitation experiments demonstrated the interaction between ID3 and LRP6 in CECs. (C)Representative western blot analysis of proteins LRP6 and β-catenin. (D) Statistical analysis of (n = 3). (E) Representative immunofluorescent staining of β-catenin (red) and DAPI (blue) in human CECs. Bars = 50 μm. * versus CON group, # versus HSV-1 + NC group *$p < 0.05$; **$p < 0.01$; ***$p < 0.001$; ****$p < 0.0001$ and ^{ns} $P > 0.05$

4. Discussion

To elucidate the mechanisms of HSV-1 infection in CECs and identify new therapeutic targets, we focused on the role of ROS in viral replication. Our data show that HSV-1 infection elevates ROS levels in CECs both in *vivo* and in *vitro* models. The antioxidant NAC reduced ROS accumulation and suppressed HSV-1 replication in infected CECs. We also observed that increased ROS downregulates ID3 expression, while ID3 overexpression conversely diminishes ROS levels and inhibits HSV-1 replication. These results indicate that ROS facilitates HSV-1 replication through the ID3/Wnt signaling pathway in CECs.

It has been confirmed that HSV-1 infection can led to an increase in ROS levels in various host cells[14]. During the onset of viral keratitis, after the corneal epithelial cells are infected with HSV-1, the level of ROS within the cells significantly increases[14]. ROS is upregulated in HSV-1 infected corneal epithelial cells can cause cell damage through the activation of the p38 MAPK signaling pathway[28]. Mitochondrial dysfunction, mitochondrial autophagy and autophagy impairment may be important causes for the production of ROS in host cells infected by HSV-1[14, 29]. In our study, we found that the level of ROS was significantly upregulated in CECs infected with HSV-1.

The role of ROS in inhibiting the replication of HSV-1 within host cells remains unclear. ROS can promote the replication of HSV-1 through NF-κB activation[10]. Ferroptosis inhibitor (Fer-1) can inhibit HSV-1 replication by preventing virus-induced ROS accumulation in human astrocytoma cell line[30].Interestingly, some drugs can inhibit the replication of HSV-1 by inducing the generation of ROS within the cells[31, 32]. However, studies have shown that the ROS scavenger molecule NAC, while reducing the level of ROS in host cells, is unable to effectively inhibit the replication of HSV-1[33]. In human gastric cancer cell lines, adding NAC after HSV-1 infection can promote the replication of the virus in the host cells[34]. In our study, we found that the use of the antioxidant NAC could significantly inhibit the replication of HSV-1 in corneal epithelial cells. In fact, previous studies have also confirmed that in the host cells infected by HSV-1, the impact of ROS on viral replication shows a high degree of cell type specificity[35].

ID3 is closely related to the generation of ROS and the antioxidant process. ROS are usually important signaling molecules that induce the expression of ID3, especially under oxidative stress conditions[23]. The expression of ID3 can, in turn, affect the cell's response to oxidative stress, possibly influencing

intracellular ROS homeostasis and cell fate through regulating antioxidant defense, inflammatory response, cell survival/death signaling pathways, and other pathways[36–39]. In our study, we found that the expression level of ID3 decreased in the CECs infected by HSV-1. After the administration of NAC, the expression level of ID3 increased. Our research also found that overexpression of ID3 led to a reduction in HSV-1 replication and a decrease in ROS expression in CECs infected with HSV-1. Interestingly, ID3 is a tumor suppressor, in part because it triggers apoptosis[40].In our study, we demonstrated that ID3 suppresses the replication of HSV-1 while failing to induce an increase in the apoptosis of corneal epithelial cells.

The PI3K/Akt signaling pathway is an important signaling pathway that regulates Wnt/β-catenin[41]. Akt signaling stimulated the Wnt/b-catenin signaling pathway by directly phosphorylating b-catenin on serine 552, which correlates with increased b-catenin dependent trasncription [42] [43]. PI3K-AKT pathway inhibition also has been found as a novel host-directed antiviral mechanism against HSV-1[44]. The activation of the Wnt/β-catenin pathway has been confirmed to promote the replication of HSV-1 in trigeminal ganglion cells, lung fibroblasts and corneal epithelial cells [45–47]. In our previous study, we found that the active Wnt/β-catenin signaling pathway in HUVECs can promote the corneal neovascularization in HSK[25].In another study, we found that SGK1 expression was upregulated by activated PI3K/SGK1 signaling pathway in HSV-1 infected CECs[24]. Additionally, SGK1 activated Wnt/β-catenin signaling pathway to promote HSV-1 replication and cause CEC apoptosis[24]. However, the regulation of β-catenin by ID3 in host cells infected with HSV-1 remains unclear. In the present study, β-catenin expression and HSV-1 replication were inhibited by overexpression of ID3. These results indicate that ID3 can inhibit HSV-1 replication in CECs via the ID3/Wnt/β-catenin pathway. ID3 is a key downstream target gene of the Wnt/β-catenin signaling pathway[48], and its expression product may also exert feedback regulation on the Wnt signaling pathway itself or its downstream effects[26]. Consistent with our previous studies, we found that in HSV-1-infected corneal epithelial cells, the Wnt/β-catenin signaling pathway was activated, and the expression level of ID3 was downregulated. After overexpressing ID3, the Wnt/β-catenin signaling pathway was inhibited, and at the same time, the replication of HSV-1 and the rate of apoptosis was significantly reduced in CECs. These studies suggest that ID3 regulates the Wnt/β-catenin signaling pathway, thereby enabling HSV-1 to replicate in CECs.

During HSV-1 infection in CECs, we observed a significant increase in ROS levels. This elevated ROS downregulated ID3 expression. ID3 subsequently inhibited HSV-1 replication in corneal epithelial cells by suppressing the Wnt signaling pathway. Our findings confirm that ID3 functions as a regulatory molecule at the intersection of the ROS and Wnt/β-catenin pathways (Fig. 6). This work offers new insights for further research into HSV-1 infection in CECs.

ID3 inhibits the pathogenesis of viral keratitis through the ROS/ ID3/Wnt signaling axis.

Declarations

Declaration of competing interest

The authors declare that the research was conducted without any commercial or financial relationships that could be construed as a potential conflict of interest.

Author contributions

Na Chen: Writing original draft, Validation, Formal analysis, Visualization, Software, Methodology. Wenzhe Wang and Jie Yin: Methodology, Conceptualization, Data curation. Yue Wang and Yumeilan Liu: Investigation, Formal analysis. Huanhuan Xu and Hu Meng: Methodology, Project administration, Resources. Wei Ye and Yirui Ge: Methodology, Writing –review & editing, Funding acquisition, Resources, Supervision, Project administration.

Funding

Financial support is acknowledged from the Postdoctoral Station of Nanjing Jinling Hospital, (#49143). Jinling Hospital foundation project (2023JCYJYB133).

Acknowledgements

We want to thank Huameng Zhang from the college of plant protection at Nanjing Agricultural University provides us with Laser Scanning Confocal Microscope (LSM 980, Carl Zeiss Microscopy GmbH, Germany).

References

1. Whitley, R.J. and B. Roizman, Herpes simplex virus infections. Lancet, 2001. 357(9267): p. 1513-8.
2. Gupta, R., T. Warren and A. Wald, Genital herpes. Lancet, 2007. 370(9605): p. 2127-37.
3. Harfouche, M., et al., Estimated global and regional incidence and prevalence of herpes simplex virus infections and genital ulcer disease in 2020: mathematical modelling analyses. Sex Transm Infect, 2025. 101(4): p. 214-223.
4. Birkmann, A. and R. Saunders, Overview on the management of herpes simplex virus infections: Current therapies and future directions. Antiviral Res, 2025. 237: p. 106152.
5. Rowe, A.M., et al., Herpes keratitis. Prog Retin Eye Res, 2013. 32: p. 88-101.
6. Labetoulle, M., et al., Incidence of herpes simplex virus keratitis in France. Ophthalmology, 2005. 112(5): p. 888-95.
7. Lobo, A.M., A.M. Agelidis and D. Shukla, Pathogenesis of herpes simplex keratitis: The host cell response and ocular surface sequelae to infection and inflammation. Ocul Surf, 2019. 17(1): p. 40-49.
8. Labib, B.A. and D.I. Chigbu, Clinical Management of Herpes Simplex Virus Keratitis. Diagnostics (Basel), 2022. 12(10).
9. Wald, A., et al., Helicase-primase inhibitor pritelivir for HSV-2 infection. N Engl J Med, 2014. 370(3): p. 201-10.

10. Kim, B., et al., Ginsenoside Rg5, a potent agonist of Nrf2, inhibits HSV-1 infection-induced neuroinflammation by inhibiting oxidative stress and NF-kappaB activation. J Ginseng Res, 2024. 48(4): p. 384-394.
11. Kuang, S., et al., HSV-1 hijacks mitochondrial dynamics: potential molecular mechanisms linking viral infection to neurodegenerative disorders. Apoptosis, 2025.
12. Kwon, E.B., et al., Korean Chestnut Honey Suppresses HSV-1 Infection by Regulating the ROS-NLRP3 Inflammasome Pathway. Antioxidants (Basel), 2023. 12(11).
13. Kavouras, J.H., et al., Herpes simplex virus type 1 infection induces oxidative stress and the release of bioactive lipid peroxidation by-products in mouse P19N neural cell cultures. J Neurovirol, 2007. 13(5): p. 416-25.
14. Chang, J., et al., JAG1 mediates apoptosis in herpes simplex keratitis by suppressing autophagy via ROS/JAG1/NOTCH1/pULK1 signaling pathway. Cell Biol Toxicol, 2024. 41(1): p. 1.
15. Manivanh, R., et al., Herpes Simplex Virus 1 ICP34.5 Alters Mitochondrial Dynamics in Neurons. J Virol, 2020. 94(14).
16. Yoo, J.Y., et al., Bortezomib Treatment Sensitizes Oncolytic HSV-1-Treated Tumors to NK Cell Immunotherapy. Clin Cancer Res, 2016. 22(21): p. 5265-5276.
17. Kee, Y. and M. Bronner-Fraser, To proliferate or to die: role of Id3 in cell cycle progression and survival of neural crest progenitors. Genes Dev, 2005. 19(6): p. 744-55.
18. Ko, M., et al., E2A/HEB and Id3 proteins control the sensitivity to glucocorticoid-induced apoptosis in thymocytes by regulating the SRG3 expression. J Biol Chem, 2004. 279(21): p. 21916-23.
19. Li, H., et al., ID3 mediates the TGF-beta1-induced suppression of matrix metalloproteinase-1 in human granulosa cells. FEBS J, 2019. 286(21): p. 4310-4327.
20. Arianti, R., et al., Upregulation of inhibitor of DNA binding 1 and 3 is important for efficient thermogenic response in human adipocytes. Sci Rep, 2024. 14(1): p. 28272.
21. Owens, A.R., et al., Angiotensin II induces a region-specific hyperplasia of the ascending aorta through regulation of inhibitor of differentiation 3. Circ Res, 2010. 106(3): p. 611-9.
22. Felty, Q. and N. Porther, Estrogen-induced redox sensitive Id3 signaling controls the growth of vascular cells. Atherosclerosis, 2008. 198(1): p. 12-21.
23. Trabosh, V.A., et al., UVB upregulates the bax promoter in immortalized human keratinocytes via ROS induction of Id3. Exp Dermatol, 2009. 18(4): p. 387-95.
24. Ye, W., et al., SGK1 mediates herpes simplex keratitis via the PI3K/SGK1/ Wnt signaling pathways. Cell Signal, 2025. 127: p. 111566.
25. Wang, W., et al., METTL3-mediated m(6)A RNA modification promotes corneal neovascularization by upregulating the canonical Wnt pathway during HSV-1 infection. Cell Signal, 2023. 109: p. 110784.
26. Huang, L., et al., ID3 Promotes Stem Cell Features and Predicts Chemotherapeutic Response of Intrahepatic Cholangiocarcinoma. Hepatology, 2019. 69(5): p. 1995-2012.

27. Bergmann, S., et al., Spatial profiling of early primate gastrulation in utero. Nature, 2022. 609(7925): p. 136-143.
28. Wan, S., et al., Dot1l Aggravates Keratitis Induced by Herpes Simplex Virus Type 1 in Mice via p38 MAPK-Mediated Oxidative Stress. Oxid Med Cell Longev, 2021. 2021: p. 6612689.
29. Zhang, L., Y. Qin and M. Chen, Viral strategies for triggering and manipulating mitophagy. Autophagy, 2018. 14(10): p. 1665-1673.
30. Xu, X.Q., et al., Herpes Simplex Virus 1-Induced Ferroptosis Contributes to Viral Encephalitis. mBio, 2023. 14(1): p. e0237022.
31. Qiu, M., et al., Pyrrolidine dithiocarbamate inhibits herpes simplex virus 1 and 2 replication, and its activity may be mediated through dysregulation of the ubiquitin-proteasome system. J Virol, 2013. 87(15): p. 8675-86.
32. Chen, X., et al., Inhibition of herpes simplex virus infection by oligomeric stilbenoids through ROS generation. Antiviral Res, 2012. 95(1): p. 30-6.
33. Luo, Z., et al., Inhibitory effects of baicalein against herpes simplex virus type 1. Acta Pharm Sin B, 2020. 10(12): p. 2323-2338.
34. Stanziale, S.F., et al., Infection with oncolytic herpes simplex virus-1 induces apoptosis in neighboring human cancer cells: a potential target to increase anticancer activity. Clin Cancer Res, 2004. 10(9): p. 3225-32.
35. Marino-Merlo, F., et al., NF-kappaB-Dependent Production of ROS and Restriction of HSV-1 Infection in U937 Monocytic Cells. Viruses, 2019. 11(5).
36. Clutter, E.D., et al., Inhibitor of DNA-Binding 3 Is a Novel Regulator of Limbal Epithelial Cell Migration Via the EphA2/Akt Signaling Pathway. Invest Ophthalmol Vis Sci, 2025. 66(9): p. 2.
37. Tan, X., et al., Reprogramming of skin fibroblasts by 3D spheroid culture promotes peripheral nerve regeneration via the ID3/semaphorin7a pathway. Stem Cells Transl Med, 2025. 14(3).
38. Koyama, T., et al., Id3-mediated enhancement of cisplatin-induced apoptosis in a sarcoma cell line MG-63. Anticancer Res, 2004. 24(3a): p. 1519-24.
39. Nickenig, G., et al., Redox-sensitive vascular smooth muscle cell proliferation is mediated by GKLF and Id3 in vitro and in vivo. FASEB J, 2002. 16(9): p. 1077-86.
40. Nagasaka, M., et al., ID3 is a novel target gene of p53 and modulates lung cancer cell metastasis. Biochemical and biophysical research communications, 2024. 708: p. 149789.
41. Chen, F., et al., Inhibitor of DNA binding 3 reverses cisplatin resistance in human lung adenocarcinoma cells by regulating the PI3K/Akt pathway. Oncology letters, 2018. 16(2): p. 1634-1640.
42. Zhao, S., et al., Activation of Akt/GSK-3beta/beta-catenin signaling pathway is involved in survival of neurons after traumatic brain injury in rats. Neurological research, 2012. 34(4): p. 400-407.
43. Lee, G., et al., Phosphoinositide 3-kinase signaling mediates beta-catenin activation in intestinal epithelial stem and progenitor cells in colitis. Gastroenterology, 2010. 139(3): p. 869-881.e8819.

44. Lee, G., et al., Phosphoinositide 3-kinase signaling mediates beta-catenin activation in intestinal epithelial stem and progenitor cells in colitis. Gastroenterology, 2010. 139(3): p. 869-881.e8819.
45. Zhu, L. and C. Jones, The canonical Wnt/beta-catenin signaling pathway stimulates herpes simplex virus 1 productive infection. Virus Res, 2018. 256: p. 29-37.
46. Harrison, K.S. and C. Jones, Wnt antagonists suppress herpes simplex virus type 1 productive infection. Antiviral Res, 2021. 191: p. 105082.
47. Koujah, L., et al., Heparanase-Induced Activation of AKT Stabilizes beta-Catenin and Modulates Wnt/beta-Catenin Signaling during Herpes Simplex Virus 1 Infection. mBio, 2021. 12(6): p. e0279221.
48. Ouchi, Y., et al., beta-Catenin signaling regulates the timing of cell differentiation in mouse retinal progenitor cells. Mol Cell Neurosci, 2011. 46(4): p. 770-80.

Figures

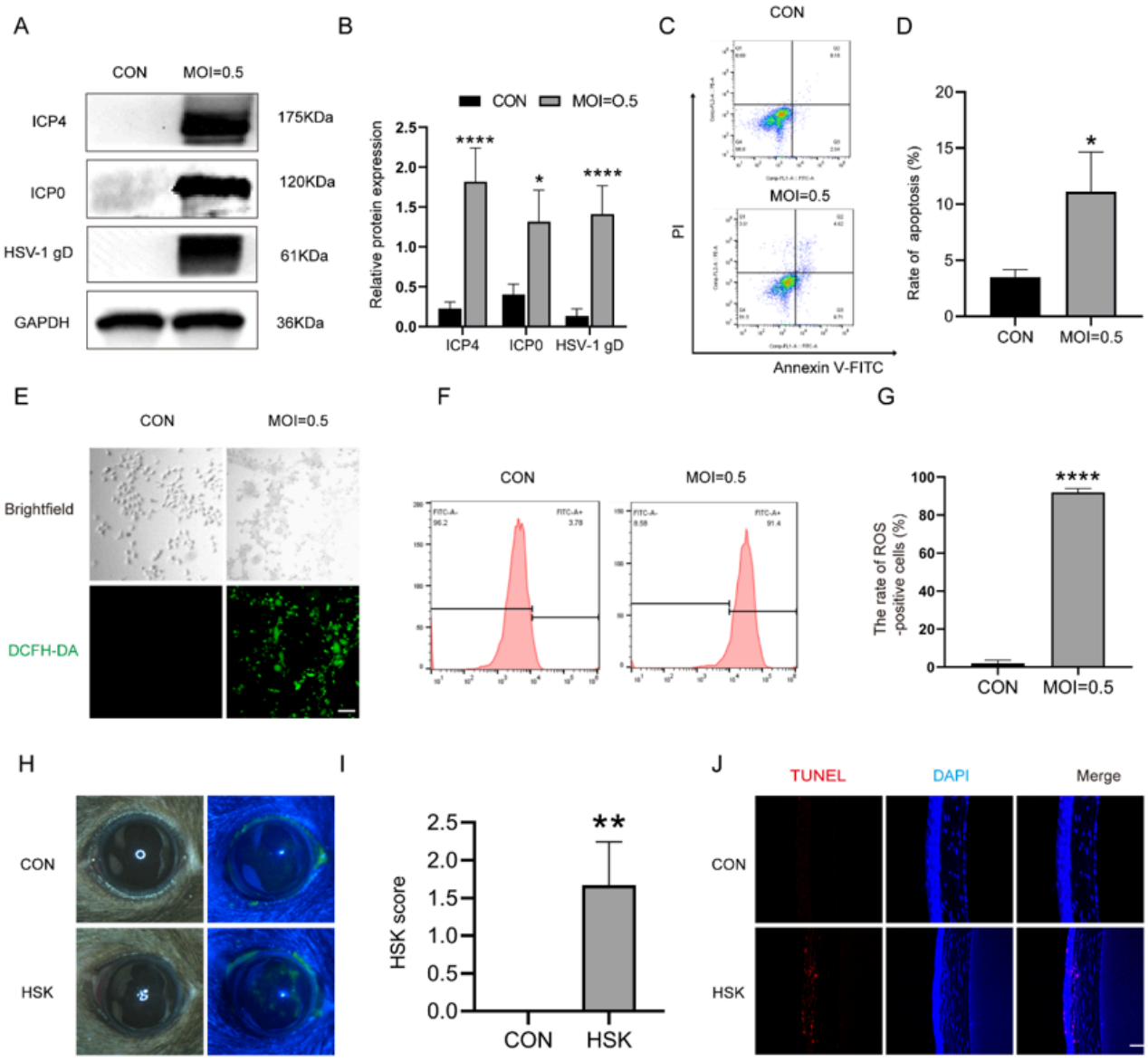


Figure 1

ROS level and apoptosis of the cornea epithelial cells increased after infected by HSV-1 in *vitro and in vivo*.

(A–G) Human CECs were infected by HSV-1(MOI = 0.5) for 24 h. (A) Representative western blot showing ICP4, ICP0 and HSV-1 gD protein expression. (B) Statistical chart of A (n = 3). (C) Flow cytometry staining results of apoptosis. (D) Statistical chart of B (n = 3). (E) Representative immunofluorescence staining by DCFH-DA (bars =100 μm). (F) Flow cytometry staining results of ROS generation. (G) Statistical chart of F (n= 3). (H) Typical images of mice corneal and fluorescein sodium staining images taken on 3 dpi. (I) Statistical chart of HSK score (n = 3). (J) TUNEL staining of mice corneal sections on 3 dpi. TUNEL staining (red) and DAPI (blue). Bars = 100 μm. *P < 0.05, **P < 0.01, ***P < 0.001 and ****P< 0.0001 versus the CON group.

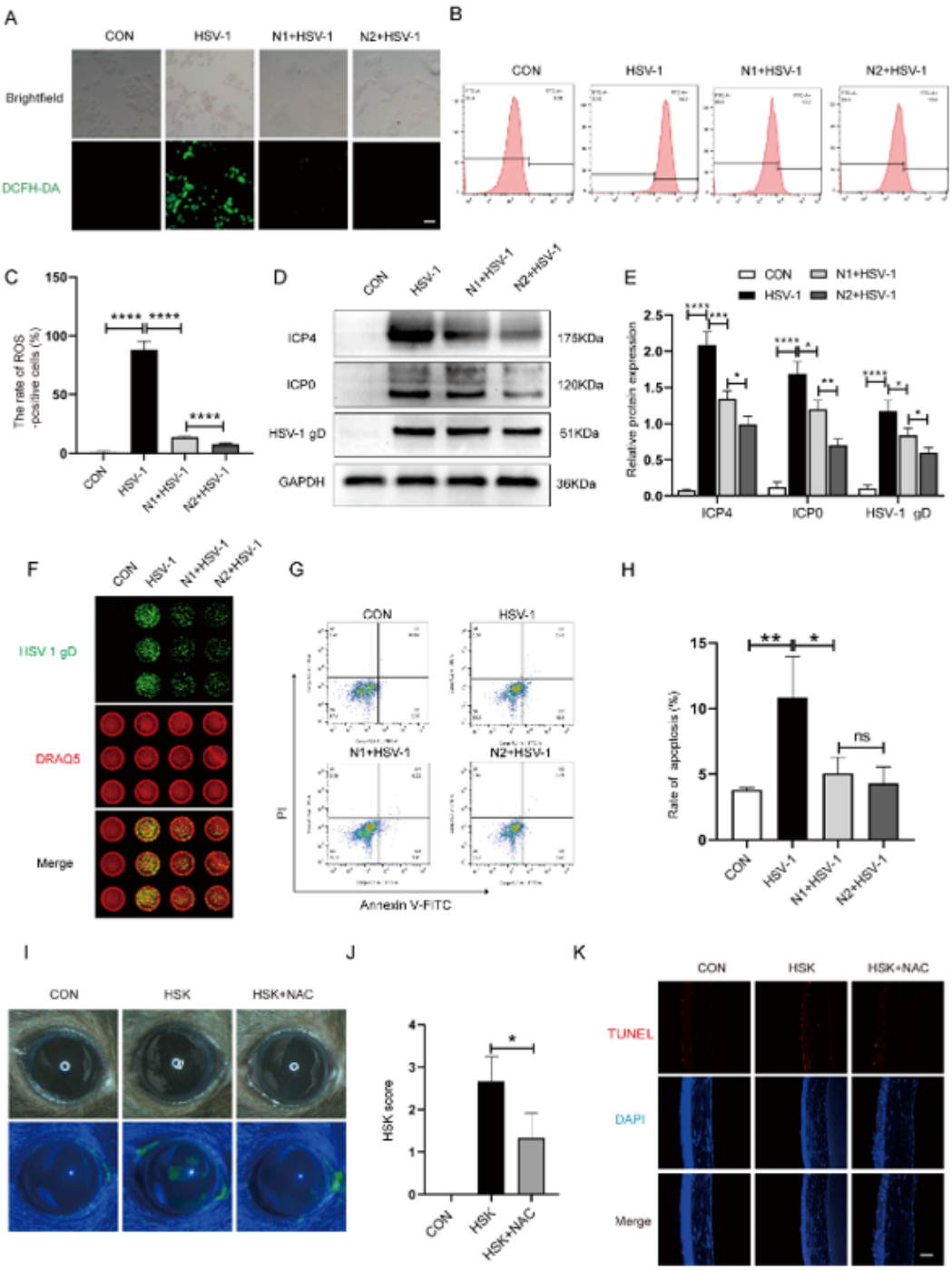


Figure 2

NAC can inhibit HSV-1 replication, ROS level and apoptosis of HSV-1 infected CECs in *vitro* and in *vivo*

(A–G) Human CECs were infected by HSV-1(MOI = 0.5) for 24 h. Human CECs were pretreated by different concentration of NAC (N1= 5 Mm and N2=10 Mm), then HSV-1 infected human CECs for 24 hours. (A) Representative immunofluorescence staining by DCFH-DA (bars =100 μm). (B) Flow cytometry

staining results of ROS generation. (C) Statistical chart of B (n= 3). (D) Representative western blot showing ICP4, ICP0 and HSV-1 gD protein expression. (E) Statistical chart of D (n = 3). (F) In cell western blot analysis was used to identify the viral protein HSV-1 gD (green), which was normalized by DRAQ5 (red). (G) Flow cytometry staining results of apoptosis. (H) Statistical chart of G (n = 3). (I-K) Mice in the NAC group were treated with NAC eye drops (0.3%, 5 μL/ eye, three times daily) for 3 continuous days (I) Typical images of mice corneal and fluorescein sodium staining images taken on 3 dpi. (J) Statistical chart of HSK score (n = 3). (K) TUNEL staining of mice corneal sections on 3 dpi. TUNEL staining (red) and DAPI (blue). Bars = 100 μm. *P < 0.05, **P < 0.01, ***P < 0.001 and ****P < 0.0001.

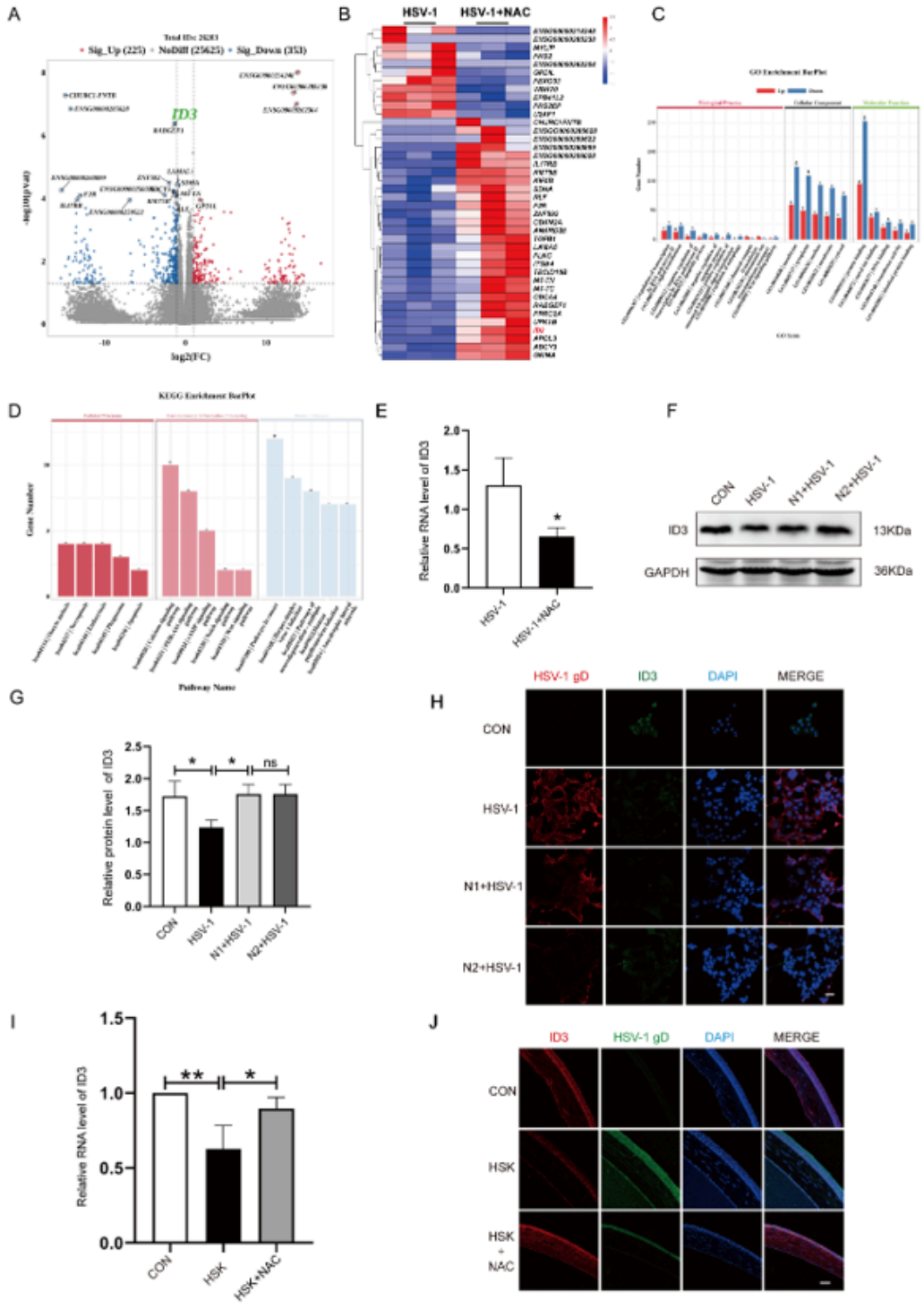


Figure 3

ID3 expression in CECs and corneal tissues after infected with HSV-1 and treated by NAC

Whole transcriptome sequencing between the HSV-1(MOI = 0.5)-infected and 5 Mm NAC pretreated HSV-1(MOI = 0.5) infected group at 24 hpi. (A–J) Whole transcriptome sequencing between the HSV-1(MOI = 0.5)-infected and 5 Mm NAC pretreated HSV-1(MOI = 0.5) infected group at 24 hpi. (A) Volcano

plot of whole transcriptome sequencing data, upregulated genes (red) while downregulated genes (blue) Grey non-significantly different (Grey). (B) Heat map of different expression genes clustering. Red indicates upregulation, and blue indicates downregulation. (C) Scatter plot of GO for different expression genes in different classifications. (D) Bar plot of KEGG enrichment pathway. (E) Relative expression of ID3 mRNA level (n = 3). (F) Representative western blot showing the ID3 protein expression. (G) Statistical chart of F. (H) Representative immunofluorescent staining of HSV-1 gD (red), ID3 (green) and DAPI (blue) in human CECs. Bars = 50 μm. (I) Relative expression of ID3 mRNA level in mice cornea (n = 3). (J)Immunofluorescent staining of ID3 (red), HSV-1 gD (green) and DAPI (blue) of mice corneal tissues. Bars = 100 μm.$^{**}P < 0.05$, $^{**}P < 0.01$ and $^{ns}P > 0.05$.

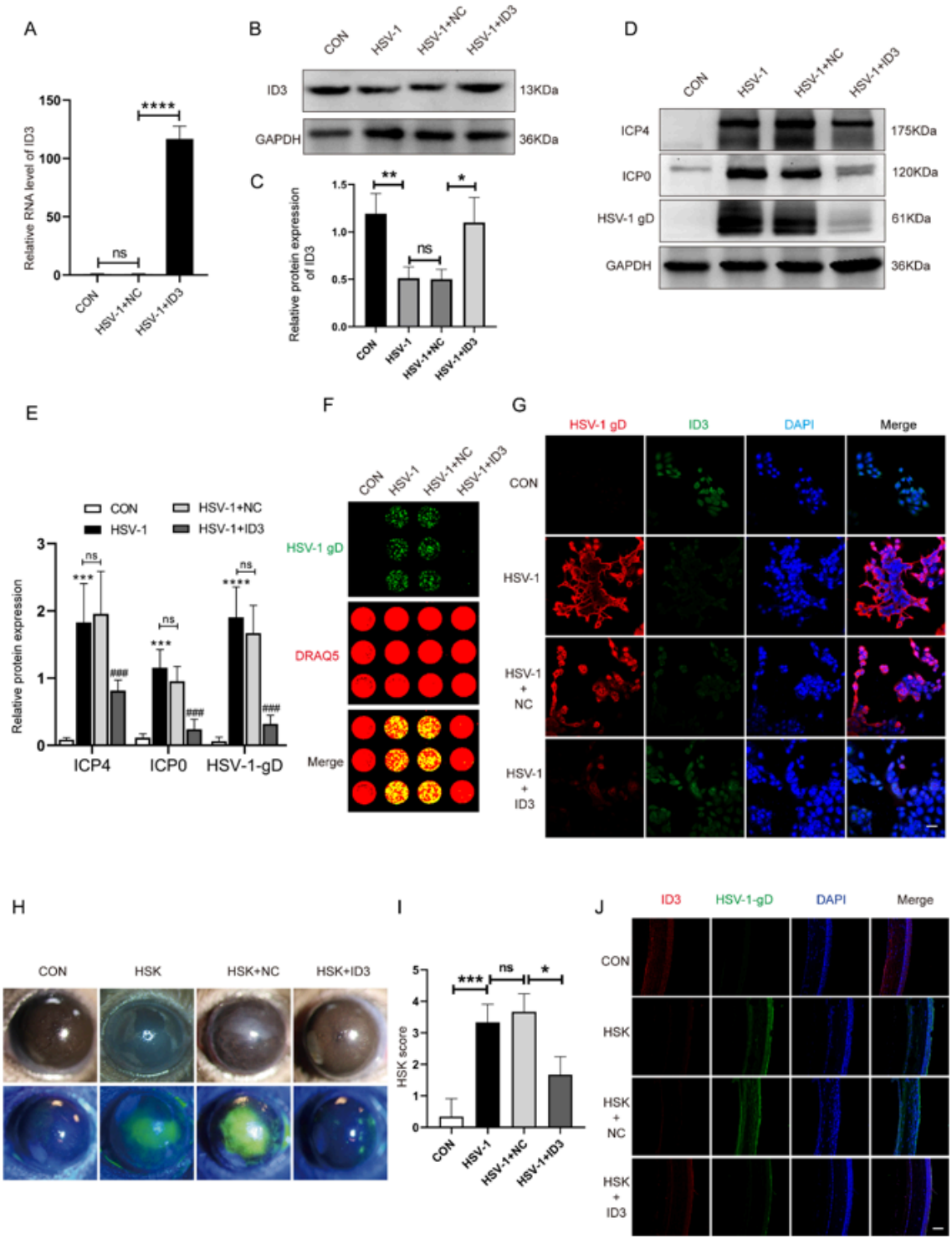


Figure 4

ID3 overexpression can inhibit the replication of HSV-1 in CECs

(A-I) ID3 was overexpressed in human CECs using plasmids. (A)Relative mRNA levels of ID3 (n = 3). (B) Representative western blot showing ID3 protein expression. (C) Statistical chart of B (n = 3). (D) Representative western blot showing ICP4, ICP0 and HSV-1 gD protein expression. (E) Statistical chart of

D (n = 3). (F) In cell western blot analysis was used to identify the viral protein HSV-1 gD (green), which was normalized by DRAQ5 (red). (G) Representative immunofluorescent staining of HSV-1 gD (red), ID3 (green) and DAPI (blue) in human CECs. Bars = 50 μm. (H) Typical images of mice corneal and fluorescein sodium staining images taken on 3 dpi. (I) Statistical chart of HSK score (n = 3).(J) Immunofluorescent staining of ID3 (red), HSV-1 gD (green) and DAPI (blue) of mice corneal tissues. Bars = 100 μm.. * versus CON group, # versus HSV-1+NC group *$p < 0.05$; **$p < 0.01$; ***$p < 0.001$; ****$p < 0.0001$ and ^{ns} $P>0.05$.

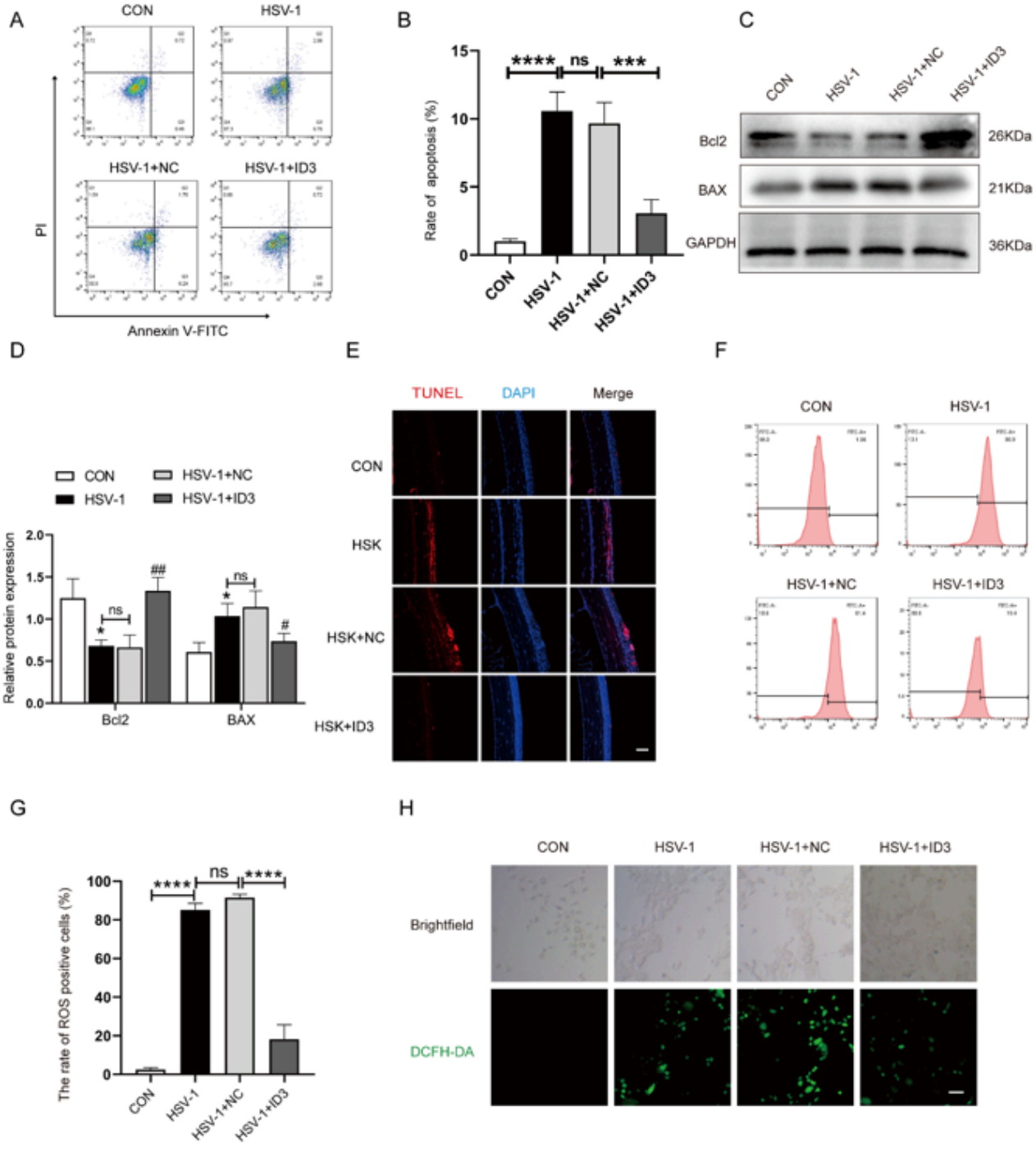


Figure 5

ID3 overexpression can inhibit apoptosis and ROS level in CECs

(A) Flow cytometry staining results of apoptosis in CECs. (B) Statistical chart of A (n= 3). (C) Representative western blot analysis of apoptosis-related proteins BAX and Bcl-2. (D) Statistical analysis of (n = 3). (E) TUNEL staining of mice corneal sections on 3 dpi. TUNEL staining (red) and DAPI (blue). Bars = 100 μm. (F) Flow cytometry staining results of ROS generation. (G) Statistical chart of F (n = 3). (H) Representative immunofluorescence staining by DCFH-DA (bars =100 μm). * versus CON group, # versus HSV-1+NC group *$p < 0.05$; **$p < 0.01$; ***$p < 0.001$; ****$p< 0.0001$ and ^{ns} $P>0.05$.

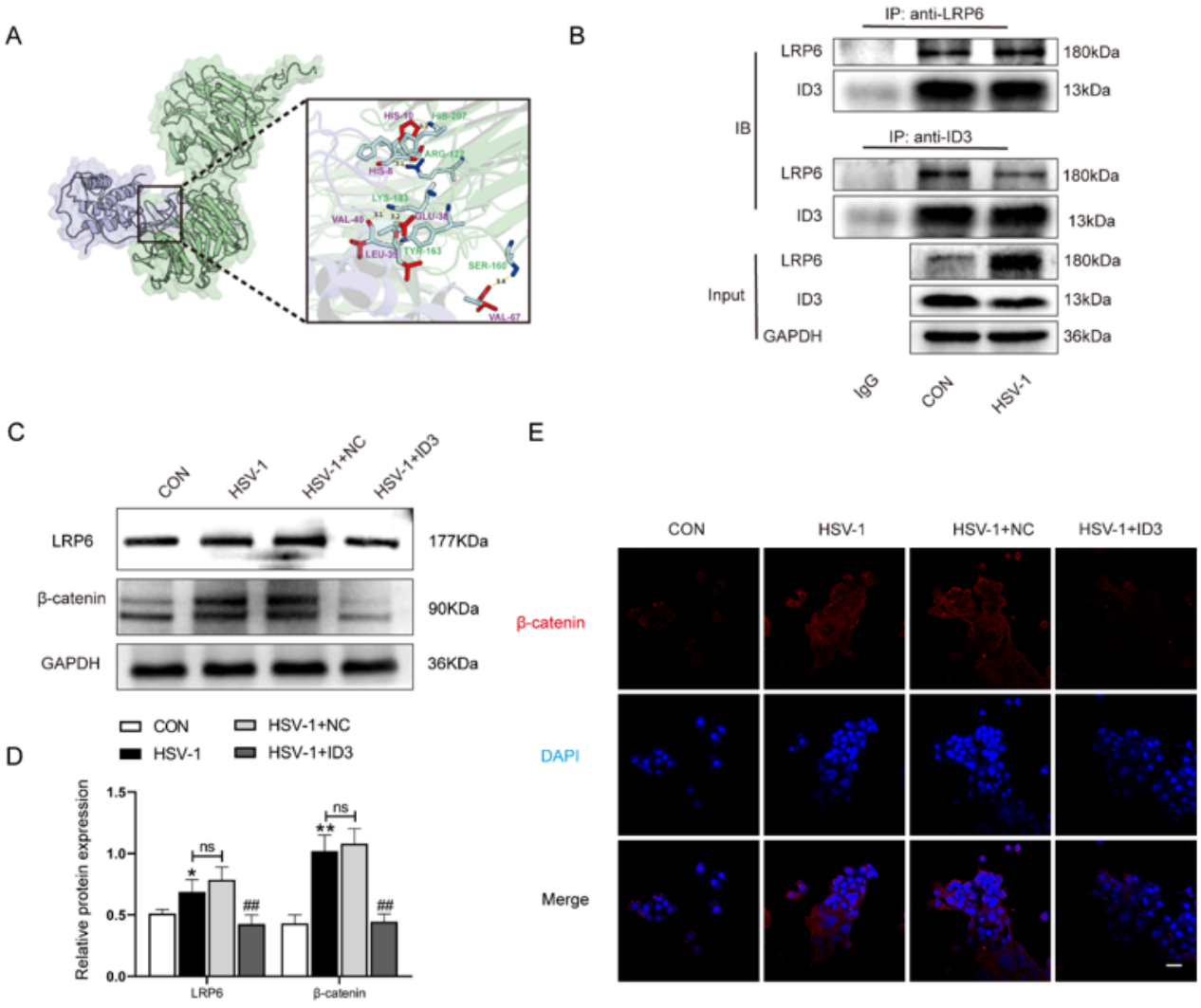


Figure 6

ID3 inhibits HSV-1 replication via the ID3/Wnt signaling pathway in CECs

(A) Three-dimensional molecular docking model of ID3 with LRP6, showing the predicted binding interface. (B) Co-IP and immunoprecipitation experiments demonstrated the interaction between ID3 and LRP6 in CECs. (C)Representative western blot analysis of proteins LRP6 and β-catenin. (D) Statistical

analysis of (n = 3). (E) Representative immunofluorescent staining of β-catenin (red) and DAPI (blue) in human CECs. Bars = 50 μm. * versus CON group, # versus HSV-1+NC group *$p < 0.05$; **$p < 0.01$; ***$p < 0.001$; ****$p < 0.0001$ and ^{ns} $P > 0.05$

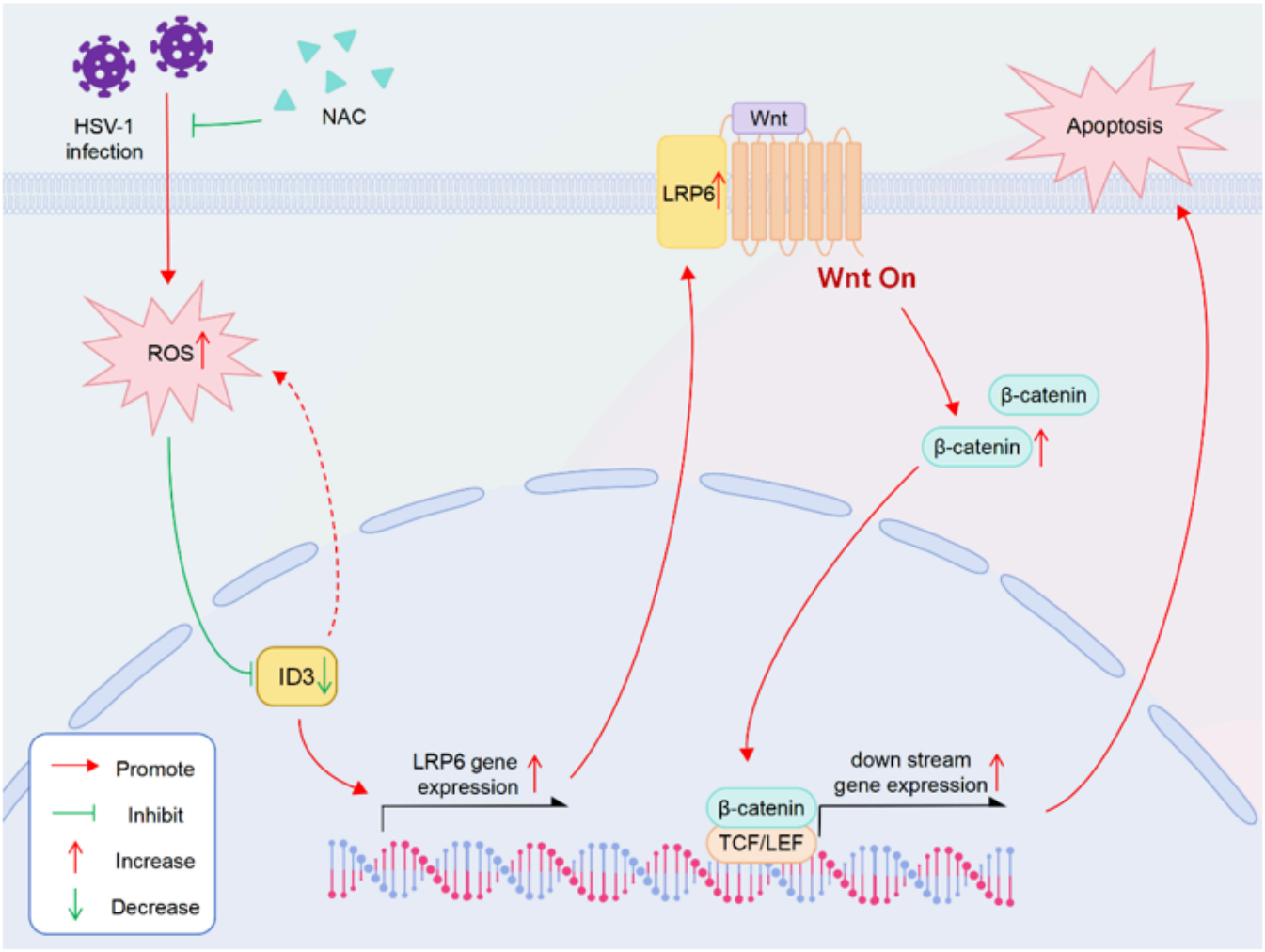


Figure 7

Diagram of research.

ID3 inhibits the pathogenesis of viral keratitis through the ROS/ ID3/Wnt signaling axis.